Impact of chemoeffectors on bacterial motility, transport and contaminant degradation in sand-filled percolation columns

CELIA JIMENEZ-SANCHEZ[†], LUKAS Y. WICK[‡] AND JOSE-JULIO ORTEGA-CALVO[*,†]

[†]*Instituto de Recursos Naturales y Agrobiología de Sevilla (IRNAS-CSIC), Avenida Reina Mercedes, 10, E-41012-Seville, Spain*

[‡]*UFZ Helmholtz Centre for Environmental Research, Permosertraße 15, D-04318 Leipzig, Germany*

Keywords: bioremediation, tactic response, bacterial transport, bacterial retention, mineralization

August 9th, 2018

[*]Corresponding author tel: (+34) 95-4624711; fax: (+34) 95-4624002; e-mail: jjortega@irnase.csic.es

20 TOC

21

22

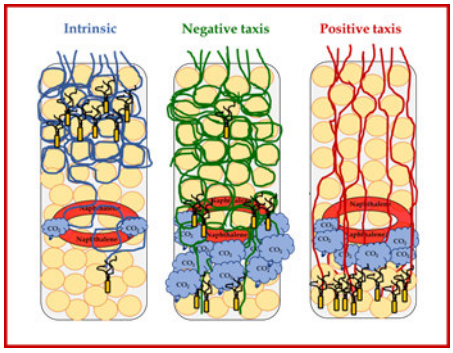

2

ABSTRACT:

Chemoeffector-mediated bacterial motility and tactic swimming are major drivers for contaminant accessibility and biodegradation at submillimeter scales. In sand-filled percolated columns we tested how and to which degree chemoeffectors influenced bacterial transport and thereby promoted accessibility and degradation of distantly located ^{14}C-naphthalene (NAH) at the centimeter scale. Sunflower root exudates and silver nanoparticles (AgNPs) were used as chemoeffectors to stimulate opposing effects of motility and tactic swimming of NAH-degrading *Pseudomonas putida* G7. Sunflower exudates prompted smooth bacterial movement and positive taxis, while AgNPs induced tortuous movement and repellent responses. Compared to chemoeffector-free controls exudates reduced deposition and stimulated bacterial transport during percolation experiments. AgNPs, however, provoked bacterial deposition and concomitant saturation of the collector surfaces (filter blocking) that led to progressively increased percolation of cells. Despite of mechanistic differences, both motility patterns supported bacterial transport and promoted mineralization rates of NAH desorbing from a source placed at the column outlet. Observed mineralization rates in presence of the chemoeffectors were fivefold higher than in their absence and similar to NAH-mineralization in well-stirred batch assays. Our results indicate that chemically mediated, small-scale bacterial motility patterns may become relevant for long-distance bacterial transport and the biodegradation of patchy contaminants at higher scales, respectively.

INTRODUCTION

Despite of the high relevance of bacterial tactic swimming for the ecology of contaminant degradation at the sub-millimeter scale,[1-6] the impact of taxis on environmental processes and applications occurring at centimeter to decimeter scale (e.g. in bioremediation and waste-water treatments) still remains elusive. Tactic reactions of flagellated bacteria are typically reflected by distinct shifts in the motility pattern due to modifications of the rotation of their flagella. Motility patterns may influence bacterial adhesion to solid surfaces; for instance, deposition of *Escherichia coli* [7, 8] and *Pseudomonas putida* [9] was favored by abrupt movements, whereas smoother and more-continuous swimming reduced adhesion of the same cells. By impelling bacterial deposition, motility may also impact bacterial transport through porous materials.[10, 11] Using NAH-degrading bacterium *Pseudomonas putida* G7 it was shown that bacterial motility and dispersal can be controlled by exposure to a suitable choice of tactic effectors. In the absence of a tactic effector, the spontaneous cell swimming strain G7 was characterized by straight or circular paths and occasional changes in the direction preventing significant long-distant transport. In the presence of chemical effectors that provoked positive tactic swimming (such as salicylate[9] or easily biodegradable dissolved organic matter (DOM) from sunflower root exudates)[12] G7 cells however showed smooth motility and poor bacterial interaction with collector surfaces. Silver nanoparticles (AgNPs) on the other hand led to induced abrupt movements, high adhesion rates, fast concomitant saturation of the collector surfaces (filter blocking) and high transport. [9] Although driven by different mechanisms (poor deposition rates *vs*. fast saturation of the collector surface) both tactic responses increased bacterial transport through porous materials. [9, 12] Still unknown remains how chemoeffector-mediated transport enables access of catabolically active bacteria to distant contaminant sources (e.g. soil aggregates and non-aqueous phase liquids (NAPLs)) and concomitant extents of contaminant biodegradation and mineralization.

Following preferential transport of a cell to the vicinity of a pollutant source [13], chemotactic

swimming may allow substrate uptake by a cell to exceed the rate of aqueous pollutant diffusion and to enhance the rate of biodegradation and mineralization.[4] High contaminant-degrading biomass in close vicinity to sources of desorbing contaminants additionally promotes contaminant mass transfer to the aqueous phase by steepening pollutant concentration gradients at the interfaces as e.g. formed by non-aqueous phase liquids (NAPLs).[5] Once the chemoeffector-mediated transport to distant pollutant sources occurs, the simultaneous tactic reactions to various stimuli is a pre-requisite for these accessibility-promoting mechanisms, because chemotaxis to dissolved pollutants should not be overridden by the effects of the other tactic effectors present in coexisting concentration gradients. However, the positive tactic response occurring with easily biodegradable DOM, such as root exudates,[12] suggests that multiple tactic responses are possible.

In this paper, we challenged the hypothesis whether chemoeffector-mediated motility patterns of the chemotactic bacterium *P. putida* G7 lead to changed centimeter-scale transport of bacteria, and, subsequently, to enhanced accessibility and mineralization of NAH as compared to situations in the absence of an effector. For this reason, sunflower root exudates and AgNPs were selected as tactic effectors to either induce smooth or abrupt motility in sand-filled percolated columns [9, 11, 12, 14] and differing transport to a ^{14}C-NAH desorbing from a source at the outflow of the column. Mineralization rates of desorbed NAH in column experiments was monitored by radiorespirometric measurements and compared to ^{14}C-NAH mineralization rates in well stirred batch systems.

MATERIAL AND METHODS

Materials

Root exudates, obtained from sunflower plants propagated in vitro, were used at 16 mg L^{-1} of total organic carbon (TOC). The procedure for obtaining the exudates and its composition is described elsewhere.[12] Silver nanoparticles (AgNPs), purchased from Sigma-Aldrich, Inc. (St. Louis, MO,

USA) were used at 0.2 mg L^{-1}.[9] Fine-grained sand was obtained from Panreac Quimica SA (Barcelona, Spain) and sieved to give a fraction between 0.40 mm and 0.25 mm diameter. Silicone rings (O-rings) were obtained from Altec Products Ltd. (Cornwall, UK) with an inner diameter of 2.57 mm and a cross section of 1.78 mm. Unlabeled NAH and ^{14}C-UL-NAH (31.3 mCi $mmol^{-1}$; radiochemical purity >98%) were purchased from Sigma Chemical Co., Steinheim, Germany.

Cultivation of bacteria

NAH-degrading soil bacterium *Pseudomonas putida* G7 was cultivated and prepared as described elsewhere. [9] Strain G7 is motile by means of polar flagella and exhibits positive taxis towards NAH and sunflower root exudates, and negative taxis towards silver nanoparticles.[9, 12] In all experiments, strain G7 was grown in an inorganic salts solution (MM) using sodium salicylate (5 mM) as carbon source.[9] Liquid cultures were performed in 250 mL-Erlenmeyer flasks containing 100 mL of MM with sodium salicylate. Bacterial cultures were maintained under continuous agitation (150 rpm) at 30 °C. At early stationary phase (48 hours after inoculation of the culture; OD_{600nm} of 0.5 (5 x10^8 cells mL^{-1}), cells were centrifuged for 10 minutes at 1000 g and re-suspended in mineral medium (MM) supplemented with or without tactic effectors. The centrifuge speed was selected to avoid breakage of flagella and thus loss of motility. The microbial biomass was estimated by the quantification of the total protein by the Lowry method.[15]

Dynamic doping of ^{14}C-NAH containing materials

The dynamic doping method was used to load the O-rings with ^{14}C-NAH.[16] A maximum of 8 rings were placed on the bottom of a 20 mL-glass tube and 1 mL of an acetone solution of ^{14}C-NAH and sufficient unlabeled NAH to give a concentration of 50 mg L^{-1} was added. The solution contained the required radioactivity to make each ring to be loaded with approximately 200,000 dpm. The tube was left opened overnight in a fume-hood to allow the complete evaporation of the acetone. To help the homogenous incorporation of NAH into the silicone, drops of milli-Q water were then applied. [16] Due to the moderate volatility of NAH that eventually led to losses of the compound

during loading the amount of NAH present in the loaded rings was determined separately. For this aim, two loaded rings were separately placed in a glass vial and 1 mL of methanol was added. After 72 hours of extraction, ^{14}C-NAH present in the methanol extracts was measured by liquid scintillation. The total amount of NAH initially present in each ring was 6.25 µg for column experiments with control cells and AgNPs and 8.30 µg for experiments with exudates.

Batch adhesion and mineralization experiments

Adhesion experiments

Adhesion experiments were performed in duplicate with sand or O-rings to check the bacterial affinity to these materials used in a non-flowing system. In brief, 20 mL glass vials containing 1.5 g of sand or 23 rings (which corresponded to 1.5 g of material) and 1 mL of the test cell suspension (OD_{600nm} of ~0.3, 10^8 cells mL^{-1}) were maintained in an orbital shaker at 80 rpm at room temperature. Attachment was determined as a percentage of the initial OD in the cell suspension after 30 min of incubation. Significant differences between treatments were analyzed using ANOVA test, Tukey HSD, $P \leq 0.05$, using SPSS 11.5 (SPSS, Chicago, IL, USA).

Mineralization experiments

Batch mineralization experiments were performed in 10-mL test tubes with 5 mL of a bacterial suspension in MM with the dissolved chemical effectors. Approximately 20,000 dpm of labeled NAH and unlabeled NAH to give a final concentration of 10 µg mL^{-1} was completely dissolved in the bacterial suspension (OD_{600nm} of ~0.3, 10^8 cells mL^{-1}). The aqueous solubility of NAH is 30 µg mL^{-1}.[11] The test tubes were closed with Teflon-lined stoppers equipped with a suspended 2-mL vial that contained 1 mL of 0.5 M NaOH and were maintained at 23 ± 2 °C on an orbital shaker operating at 150 rpm. Then, ^{14}C-NAH mineralization was measured as radioactivity incorporated in the alkali trap. The sample (1 mL) was collected from the trap and mixed with 5 mL of scintillation fluid (Ready Safe, Beckman Instruments, Fullerton, California, USA). Radioactivity was measured on a liquid scintillation counter model LS6500 Beckman (Beckman Instruments, Fullerton,

California, USA). The maximum rates (V_s, in ng μg_{prot}^{-1} min^{-1}) and extents (E_{min}, %) of $^{14}CO_2$ production were calculated as described earlier. [11]

Column transport and mineralization experiments

Bacterial transport and NAH mineralization was tested simultaneously in duplicate at 25°C in vertical (10 cm length and 0.9 cm inner diameter) percolated sand columns with an porosity (estimated gravimetrically) of 0.34, corresponding to a pore volume (PV) of 2.3 mL.[9, 12] Silicone rings (O-rings), containing sorbed ^{14}C-NAH (cf. above), were placed two centimeters from the outlet of the columns to simulate a distant NAH source (cf. Figure S1). Each ring was collected with forceps and washed separately in milli-Q water before being introduced (once dried with blotting paper) to the column. Bacterial suspensions (OD_{600nm} = 0.3, i.e. ca. 10^8 cells mL^{-1}) were pumped through the columns at a constant flow rate of 0.135 ± 0.02 mL min^{-1} (hydraulic flow rate 0.50 cm min^{-1}). The column effluent was collected every 20 minutes into 20 mL test tubes in order to photometrically measure cell concentrations. The total radioactivity and $^{14}CO_2$ produced was also measured by liquid scintillation counting as detailed below. The column breakthrough of the bacteria was followed by comparing the OD_{600nm} of the influent (C_0) and effluent (C) at given time intervals. The breakthrough curves also allowed us to calculate the percolated biomass (X_{sus}) and the total attached biomass (X_{att}) in the columns at given time points. These values were inferred by difference from the input and output OD measurements. Control determinations excluded any interference on OD measurements by the chemoeffectors solutions used. Based on the data of the breakthrough curves the clean-bed adhesion efficiency (α_o) and the blocking factor (B_f) was determined as previously described.[9] Shortly, α_o is defined as the ratio of the rate of bacterial attachment to the rate of bacterial transport to the collector surfaces, whereas B_f is defined as the ratio of the area of the collector blocked by a deposited particle to the area of that particle. A more detailed description of the theoretical background and calculation method for α_o and B_f can be found elsewhere. [9, 11]

166 An aliquot of the column effluent (0.5 mL) was used to measure total radioactivity by liquid
167 scintillation. This measurement was carried out to determine the total concentration of NAH
168 leached from the columns ($C_{tot,n}$). To the remaining volume, 1 mL of 2N HCl was added in order to
169 inactivate the bacterial cells and the mixture stirred at 80 rpm for 12 hours to remove and
170 incorporate $^{14}CO_2$ present in the effluent fractions in an alcali trap (cf. Figure S1). Radioactivity
171 incorporated into the trap was measured by liquid scintillation. Specific mineralization rates V_s (ng
172 μg_{prot}^{-1} min^{-1}) were calculated as described in a previous study: [14]

173 $$V_s = \frac{C_{CO2,n} V_{sample}}{X_{sus} t_{res} + X_{att} t_{sample}} \quad (1)$$

174 where $C_{CO2,n}$ is the concentration of mineralized NAH in the effluent (ng mL^{-1}), V_{sample} is the sample
175 volume (mL), X_{sus} is the biomass of suspended bacteria transported with the sample volume (µg
176 prot), t_{res} is the residence time in the column portion below the ring or exposure zone (min), X_{att} is
177 the biomass attached to the column matrix (µg prot), and t_{sample} is the sampling interval (min). Due
178 to operational limitations, some samples for $C_{CO2,n}$ measurements were not accompanied by
179 simultaneous OD determinations. In those cases, X_{sus} and X_{att} were calculated from the slope of OD
180 measurements immediately before and after the corresponding $C_{CO2,n}$ sampling point. Equation 1
181 accounts for the fact that suspended cells can mineralize NAH only during their passage through the
182 column portion exposed to NAH (i.e., desorbed from the ring), the duration of which is t_{res}. Time-
183 dependent mineralization extents E_{min} (%) were further calculated, by dividing the amount of NAH
184 appearing in the effluent as CO_2 by the accumulative amount of total NAH (C_{tot}) leached from the
185 columns up to that sampling point:

186 $$E_{\min} = \frac{\sum C_{CO2,n} V_{sample}}{\sum C_{tot} V_{sample}} x100 \quad (2)$$

187 To have comparable values, the extents of mineralization were calculated in the different column
188 experiments at the point when 1 µg of NAH had been leached from the columns (approximately at 8

PV). It should be noted that C_{tot} in eq. 2 differs from $C_{tot,n}$, which denotes the concentration of total NAH measured in each effluent sample.

RESULTS

Effect of motility patterns on bacterial adhesion and NAH mineralization in batch experiments

Bacterial motility patterns and adhesion

Batch experiments were used to study the effects of chemoeffector-induced motility patterns on adhesion to sand and silicone O-rings, and to quantify resulting effects on mineralization of NAH in well stirred system, respectively. Motility patterns were described by the number of peaks in the rate of changes in the direction higher than 1000 $^{o}s^{-1}$(RCDI; Table 1 and Figure S2). These distinctive patterns are stable upon exposure to the chemical effectors at least during 30 min. [9, 12] Abrupt movement, with a high number of turning events, was acquired by cells in reaction to repellent AgNPs. This caused higher adhesion to sand (58 %) relative to control cells (38 %) in the absence of a chemoeffector (Table 1). By contrast, smooth motility (as characterized by a low number of turning events) was found in response to sunflower exudates. These exudates provoked positive taxis in strain *P. putida* G7 and reduced its adhesion to sand surfaces (9 %, Table 1) relative to the control. Likewise, bacterial adhesion to NAH-free silicone O-rings was significantly different ($P \leq 0.05$) in the presence of AgNPs and exudates, as compared to the control, following the same trend as with sand.

NAH mineralization

Batch mineralization experiments with completely dissolved NAH demonstrated the ability of strain *P. putida* G7 to mineralize NAH in the presence of chemoeffectors. The specific mineralization rates and final extents in presence of chemoeffectors however were not statistically different (*t*-test, $P = 0.05$) to chemoeffector-free controls (Table 1). The final extents of

mineralization measured (≈40 %) were within the expected values, whereas the rest of the substrate was probably incorporated into microbial biomass or transformed to partially oxidized byproducts.[17]

Effect of motility patterns on bacterial transport and NAH mineralization in percolation column experiments

Bacterial transport

Single cell motility effects on macroscale bacterial transport and contaminant mineralization was studied in sand-filled laboratory percolation columns in presence and absence chemoeffectors. Control cells in the absence of a chemoeffector exhibited an initial adhesion efficiency (α_o) of ≈0.38, and reached final C/C_0 values of ≈0.4 after 5 PV (Table 1, Figure 1A). The calculated filter blocking factor was B_f = 0.3. The presence of AgNPs however led to high initial adhesion efficiency ($\alpha_o \approx 0.6$) yet a sharp increase of C/C_0 values after two PV (Figure 1C) likely due to progressive saturation of the collector surfaces (filter blocking; B_f = 0.7) and subsequent improved transport. [9] Low adhesion efficiencies ($\alpha_o \approx 0.18$), high bacterial transport were observed in presence of sunflower root exudates (Figure 1E, Table 1): Suspensions of exudate-exposed cells broke through at $C/C_0 \approx 0.5$ at 1 PV, and rapidly reached C/C_0 values of 0.9 at two PV likely due to the smooth cellular motility pattern of G7 cells in presence of the exudates at the low TOC used (16 mg L^{-1}), which is significantly lower than the TOC levels (above 100 mg L^{-1}) at which DOM enhances bacterial transport through competition effects with collector surfaces.[12] This was reflected by a high estimated B_f of 1.2.

NAH mineralization

The mineralization of NAH was assessed by quantifying the concentrations of total ^{14}C-NAH ($C_{tot,n}$) and the $^{14}CO_2$ concentrations in the effluent ($C_{CO2,n}$) in the effluent. Quasi steady-state effluent concentrations of total ^{14}C-NAH in chemoeffector-free columns were ≈45 ng mL^{-1} and, hence, significantly lower than the initial concentration (10 µg mL^{-1}) tested in batch mineralization

239 experiments in order to determine the maximum mineralization potential. The $^{14}CO_2$ concentrations
240 in the effluent ($C_{CO2,n}$) (expressed as ng NAH mL^{-1} mineralized, cf. Materials and Methods section)
241 increased linearly up to 8 PV reflecting increasing access of percolated bacteria to the NAH source
242 (Figure 1A). In presence of exudates (Figure 1C) similar C_{tot} (≈ 45 ng mL^{-1}) as the control and
243 AgNPs-exposed columns were observed after approximately 4 PV despite of somewhat higher
244 initial ^{14}C-NAH values (≈ 60 ng mL^{-1}). Unexpectedly however, $C_{CO2,n}$ was significantly higher in
245 presence of the AgNPs and, to a lesser extent, sunflower exudates than control cells, in spite of
246 similar steady-state concentrations of total ^{14}C-NAH (Figure 1A).

247 Whereas the $C_{CO2,n}$ values reflect the overall biodegradation process in the column, a further
248 analysis of the results was performed by combining effluent data from C_{tot}, $C_{CO2,n}$ and estimations of
249 suspended (X_{sus}) and attached (X_{att}) bacterial biomass to approximate the specific mineralization rate
250 (V_s) and mineralization extent (E_{min}; cf. eqs. 1 & 2). The results are shown in Figures 1B, 1D, and 1F,
251 and in Table 1. In control experiments X_{att} increased linearly and was higher than the suspended
252 biomass (X_{sus}; Figure 1B) as evidenced by low X_{sus}/X_{att} ratios of ≈0.1-0.3. Corresponding values of
253 V_s remained constant (V_s ≈ 0.004 ng mg_{prot} min^{-1}) and hence were about fivefold lower than V_s of
254 batch (≈ 0.02 ng mg_{prot} min^{-1}) mineralization experiments (Table 1). As X_{att} reflects the total biomass
255 in the columns (i.e. does not discriminate attached cells placed outside from cells inside the
256 exposure zone) calculated values of V_s underestimate the activity of cells exposed to NAH. Final
257 extents of NAH mineralization in column experiments (≈41 %) however were comparable to E_{min} of
258 batch experiments (≈44 %). Cells exposed to AgNPs provoked a significantly higher NAH
259 mineralization rate (V_s = 0.017 ng μg_{prot}^{-1} min^{-1}) than was observed for control cells (V_s = 0.004 ng
260 μg_{prot}^{-1} min^{-1}); a value that was similar to *Vs* of NAH mineralization of dissolved NAH by suspended
261 cells in well-stirred batch experiments (Table 1). At 8.5 PV however, V_s decreased to 0.005 ng
262 μg_{prot}^{-1} min^{-1} and was similar to V_s of control cells. Such decrease went along with a drop of the
263 initial X_{sus}/X_{att} ratio of ≈1.3 to ≈0.3 (Table 1). At 8.5 PV the mineralization extent was 79 % and

exceeded batch mineralization extents of 34 % in presence of AgNPs. The presence of sunflower exudates provoked highest X_{sus}/X_{att} ratios that dropped 6.5 (at 2.6 PV) to 1.3 (at 6.7 PV). Similar to the X_{sus}/X_{att} ratio the V_s decreased from 0.020 to 0.006 ng μg_{prot}^{-1} min^{-1}. The presence of the exudates however, did not impact mineralization extents, which were similar to E_{min} of batch experiments (≈42 %).

DISCUSSION

Effect of chemoeffectors on bacterial motility, transport and NAH mineralization

In this study we analyzed the effect of chemoeffector-induced motility patterns on bacterial transport and the accessibility and degradation of NAH in a spatially separated source. Towards this question we compared deposition and mineralization results in batch and column assays with *P. putida* G7 cells that were induced to exhibit three distinct motility patterns: intrinsic (= control cells), negative taxis, and positive taxis. The mechanistic basis for the enhancement of bacterial transport through porous materials caused by taxis-mediated swimming modes has been described elsewhere. [9, 11, 12] These studies revealed that chemoeffectors enhanced long-range transport by changes in the motility pattern of individual cells at a pore-scale rather than modifying properties of the grain surfaces or the solution, respectively. Our results extend those findings by highlighting two factors influencing the bioaccessibility of NAH in percolation columns: i) transport efficiency of bacteria towards the exposure zone and ii) deposition efficiency of bacteria at the exposure zone. Both factors were responsible, respectively, for the observed enhancements in the specific rates and extents of NAH mineralization.

Independent of their tactic effects, chemoeffectors led to about fivefold enhanced initial V_s relative to controls and were similar to V_s of NAH degradation under well-stirred batch conditions. This observation proposes that taxis-mediated motility facilitates the access of bacteria to a spatially separated NAH source despite of opposite chemoeffector effects on cellular swimming. As $C_{tot,n}$ of

289 NAH (45-60 ng mL^{-1}) in column effluents was smaller than the concentration in batch experiments,
290 significantly smaller V_s in column experiments would be expected, given an affinity constant (or
291 K_m) of NAH degradation by strain *P. putida* G7 of 130 ng mL^{-1}. [4] This reveals that our observations
292 of emerging, apparent effluent concentrations may not entirely reflect cellular exposure to
293 microscale NAH gradients forming in close vicinity to the NAH containing O-rings. Cellular
294 proximity to the NAH source allows for high NAH mass transfer, high NAH concentrations and
295 similar degradation activity of the *P. putida* G7 cells [14, 17, 21] as in well-stirred batch assays. Such
296 proximity can be promoted by chemoeffector-mediated facilitated transport of bacteria to the
297 NAH source and, eventually, by coinciding chemotactic movement along NAH gradients. [20]
298 Changing the relative presence of bacterial biomass in the NAH exposure zone thereby can explain
299 continuously decreasing V_s values observed in column experiments, as V_s depends on the biomass
300 (X_{sus} and X_{att}) and bacterial residence time (t_{res}): Given quasi similar or even increased $C_{CO2,n}$ at
301 higher PV, decreasing V_s values are the result of higher attached biomass above the NAH exposure
302 zone (eq.1). Sunflower exudates e.g. allowed mobilizing bacteria by inducing smooth motility,
303 efficient transport to and enhanced accumulation of percolated cells in the NAH exposure zone.
304 AgNP-induced negative taxis motility, by contrast, promoted both high bacterial transport to and
305 efficient deposition in the contaminant zone.

306 Increased V_s in presence of exudates may also be due to facilitated NAH desorption induced
307 by this natural dissolved organic matter.[18] However, this process is unlikely to occur: Given 16 mg
308 L^{-1} of the exudates, a log K_{oc} of NAH of 2.98 [19] and instantaneous equilibrium apparent NAH
309 aqueous concentration would increase by ≈2% only and hence be negligible. Likewise poor impact
310 of sorption of NAH to AgNPs is to be expected, given the low concentration and organic carbon
311 content of AgNPs.[9]

312 **Effect of AgNPs on NAH mineralization**

313 The unexpectedly high mineralization extent (79 % of the leached compound, Table 1) seems rather

to be result of the effects induced by AgNPs promoting negative taxis by *P. putida* G7 cells. Although we did not measure directly the deposition of bacteria in the exposure zone, we suggest, as a plausible explanation, that the spatial confinement due to increased deposition of the cells in this zone contributed to this highest NAH mineralization extent. This enhancement of pollutant biodegradation as a result of an enhanced bioavailability constitutes, therefore, a new endpoint for the interactions of *P. putida* G7 cells with AgNPs at low, sub-toxic concentrations, to be added to the repellence due to nanoparticle-specific physical effects, independent of the release of silver ions,[22, 23] and to an enhanced transport through porous materials due to collector saturation.[9] Indeed, ettachment to surfaces has been discussed as bioavailability promoting effect due to steeper contaminant concentration gradients and higher mass transfer rates of desorbing contaminants to the cells.[14, 17, 21] Such enhanced desorption may explain the high observed mineralization extents that were higher than mineralization typically observed in other experimental situations,[24] including the batch assays (≈40 %) described in this study. Attached bacteria actively assimilating NAH also produced $^{14}CO_2$, but remained in the column with biochemically incorporated ^{14}C, thus resulting in a higher fraction of mineralized NAH in the column effluents. Assuming a mineralization efficiency of ≈40 % (in accordance with batch mineralization assays), the mineralization extent in column experiments indicates that attached bacteria were responsible for a two-fold increase of NAH transformation. Alternately, bacteria sitting on the O-rings and sand grains may also have changed their mineralization efficiency, as a part of up to date unknown physiological modifications occurring in bacterial cells upon adhesion. However, the initial V_s value detected, which is the same as that of suspended cells operating in batch experiments at their maximum potential, indicated that this explanation is unlikely.

Relevance of single cell phenomena for macroscale natural attenuation processes

Our results underpin the role of cellular bacterial motility patterns (e.g. in response to chemical effectors) for natural and technically-enhanced contaminant attenuation processes: smooth motility

without changes in the direction hence would promote suspended bacterial cells to be mobilized towards the contamination source, while abrupt motility (as characterized by a high frequency in turning events) would additionally lead to bacterial retention at the vicinity of the contaminant. In the absence of an external modulator the spontaneous motility, (as characterized by occasional changes in the direction) would make it for the bacteria more difficult to access the pollutant due to a limited dispersal. This knowledge has several potential applications. The treatment of extended areas of contamination and pollutants present at a certain depth can benefit from the use of positive tactic effectors that increase the mobilization of bacterial cells towards the contamination source. Such effectors could be present, for example in certain DOC sources enriched with chemoeffectors,[12] able to promote bacterial transport at very low OC concentrations, what would not represent a risk for pollutant mobilization due to sorption to dissolved macromolecules and/or bacterial inoculants. For localized treatments in bioreactors, negative chemoeffectors would be useful in rapidly confining motile bacteria, by promoting the bacterial adhesion and retention in the contaminated matrices. In this study, we used AgNPs as a model repellent but other chemicals causing this tactic behavior, such as zero-valent iron nanoparticles,[25] could also be tested for environmental applications. Our results could be also applied in waste-water bio-treatment in fixed-bed reactors where biofilm establishment and maintenance is fundamental in the bioreactor performance. This research work could be the initial point of a research conducted to generate biotechnologically new chemoeffectors and to to use mutant strains that exhibit continuous smooth-swimming or continuous tumbling even in the absence of any chemoeffectors that could promote the specific and directed mineralization of the contaminants.

ASSOCIATED CONTENT

Supporting Information

Figures showing the experimental setting of the column system to test the bacterial mobilization,

and cell-track computer analysis of *Pseudomonas putida* G7 motility patterns in response towards chemoeffectors. This material is available free of charge via the Internet at http://pubs.acs.org.

AUTHOR INFORMATION

Corresponding author

*Phone: +34 95 4624711. Fax: +34 954624002. E-mail: jjortega@irnase.csic.es.

ACKNOWLEDGEMENTS

We thank the Spanish Ministry of Economy, Industry and Competitiveness (CGL2013-44554-R and CGL2016-77497-R), the Andalusian Government (RNM 2337) and the European Commission (LIFE15 ENV/IT/000396). This study contributes to the research topic Chemicals in the Environment (CITE) within the research program Terrestrial Environment of the Helmholtz Association.

REFERENCES

1. Witt, M. E.; Dybas, M. J.; Worden, R. M.; Criddle, C. S. Motility-enhanced bioremediation of carbon tetrachloride-contaminated aquifer sediments. *Environ. Sci. Technol.* **1999,** *33*, 2958-2964.
2. Hawkins, A. C.; Harwood, C. S. Chemotaxis of *Ralstonia eutropha* JMP134(pJP4) to the herbicide 2,4-dichlorophenoxyacetate. *Appl. Environ. Microbiol.* **2002,** *68*, 968-972.
3. Bhushan, B.; Halasz, A.; Thiboutot, S.; Ampleman, G.; Hawari, J. Chemotaxis-mediated biodegradation of cyclic nitramine explosives RDX9 HMX, and CL-20 by *Clostridium* sp EDB2. *Biochem. Biophys. Res. Commun.* **2004,** *316*, 816-821.
4. Marx, R. B.; Aitken, M. D. Bacterial chemotaxis enhances naphthalene degradation in a heterogeneous aqueous system. *Environ. Sci. Technol.* **2000,** *34*, 3379-3383.

17

5. Law, A. M. J.; Aitken, M. D. Bacterial chemotaxis to naphthalene desorbing from a nonaqueous liquid. *Appl. Environ. Microbiol.* **2003,** *69*, 5968-5973.

6. Ortega-Calvo, J. J.; Marchenko, A. I.; Vorobyov, A. V.; Borovick, R. V. Chemotaxis in polycyclic aromatic hydrocarbon-degrading bacteria isolated from coal-tar- and oil-polluted rhizospheres. *FEMS Microbiol. Ecol.* **2003,** *44*, 373-381.

7. McClaine, J. W.; Ford, R. M. Reversal of flagellar rotation is important in initial attachment of *Escherichia coli* to glass in a dynamic system with high- and low-ionic-strength buffers. *Appl. Environ. Microbiol.* **2002,** *68*, 1280-1289.

8. Frymier, P. D.; Ford, R. M.; Berg, H. C.; Cummings, P. T. 3-dimensional tracking of motile bacteria near a solid planar surface. *Proc. Natl. Acad. Sci. U.S.A.* **1995,** *92*, 6195-6199.

9. Jimenez-Sanchez, C.; Wick, L. Y.; Ortega-Calvo, J. J. Chemical effectors cause different motile behavior and deposition of bacteria in porous media. *Environ. Sci. Technol.* **2012,** *46*, 6790-6797.

10. Liu, J.; Ford, R. M.; Smith, J. A. Idling time of motile bacteria contributes to retardation and dispersion in sand porous medium. *Environ. Sci. Technol.* **2011,** *45*, 3945-3951.

11. Velasco-Casal, P.; Wick, L. Y.; Ortega-Calvo, J. J. Chemoeffectors decrease the deposition of chemotactic bacteria during transport in porous media. *Environ. Sci. Technol.* **2008,** *42*, 1131-1137.

12. Jimenez-Sanchez, C.; Wick, L. Y.; Cantos, M.; Ortega-Calvo, J. J. Impact of dissolved organic matter on bacterial tactic motility, attachment, and transport. *Environ. Sci. Technol.* **2015,** *49*, 4498−4505

13. Furuno, S.; Pazolt, K.; Rabe, C.; Neu, T. R.; Harms, H.; Wick, L. Y. Fungal mycelia allow chemotactic dispersal of polycyclic aromatic hydrocarbon-degrading bacteria in water-unsaturated systems. *Environ. Microbiol.* **2010,** *12*, 1391-1398.

14. Ortega-Calvo, J. J.; Fesch, C.; Harms, H. Biodegradation of sorbed 2,4-dinitrotoluene in a

clay-rich, aggregated porous medium. *Environ. Sci. Technol.* **1999,** *33*, 3737-3742.

15. Daniels, L.; Handson, R. S.; Philips, J. A. Chemical analysis. *Methods for General and Molecular Bacteriology;* Gerhardt, A. P., Murray, R. G. E., Wood, W. A., Krieg, N. R., Eds., ASM Press: Washington, D. C., 1994; pp 512-554.

16. Smith, K. E. C.; Rein, A.; Trapp, S.; Mayer, P.; Karlson, U. G. Dynamic passive dosing for studying the biotransformation of hydrophobic organic chemicals: microbial degradation as an example. *Environ. Sci. Technol.* **2012,** *46*, 4852-4860.

17. Ortega-Calvo, J. J.; Alexander, M. Roles of bacterial attachment and spontaneous partitioning in the biodegradation of naphthalene initially present in nonaqueous-phase liquids. *Appl. Environ. Microbiol.* **1994,** *60*, 2643-2646.

18. Tejeda-Agredano, M. C.; Mayer, P.; Ortega-Calvo, J. J. The effect of humic acids on biodegradation of polycyclic aromatic hydrocarbons depends on the exposure regime. *Environ. Pollut.* **2014,** *184*, 435-442.

19. Schwarzenbach, R. P.; Gschwend, P. M.; Imboden, D. M. *Environmental Organic Chemistry, second edition*. John Wiley & Sons: New Jersey, 2003.

20. Adadevoh, J. S. T.; Triolo, S.; Ramsburg, C. A.; Ford, R. M. Chemotaxis increases the residence time of bacteria in granular media containing distributed contaminant sources. *Environ. Sci. Technol.* **2016,** *50*, 181-187.

21. Johnsen, A. R.; Wick, L. Y.; Harms, H. Principles of microbial PAH-degradation in soil. *Environ. Pollut.* **2005,** *133*, 71-84.

22. Ortega-Calvo, J. J.; Molina, R.; Jimenez-Sanchez, C.; Dobson, P. J.; Thompson, I. P. Bacterial tactic response to silver nanoparticles. *Environ. Microbiol. Rep.* **2011,** *3*, 526-534.

23. Guo, Y.; Stärk, H. J.; Hause, G.; Schmidt, M.; Harms, H.; Wick, L. Y.; Müller, S. Heterogenic response of prokaryotes toward silver nanoparticles and ions is facilitated by phenotypes and attachment of silver aggregates to cell surfaces: heterogenic response of prokaryotes toward

AgNPs. *Cytometry* **2017**, *A 91*, 775–784.

24. Niqui-Arroyo, J. L.; Bueno-Montes, M.; Ortega-Calvo, J. J. Biodegradation of anthropogenic organic compounds in natural environments. *Biophysico-Chemical Processes of Anthropogenic Organic Compounds in Environmental Systems;* Xing, B., Senesi, N., and P.M. Huang, P.M., Eds.; IUPAC Series on Biophysico-Chemical Processes in Environmental Systems, Vol 3, John Wiley & Sons Ltd: Chichester, 2011; pp 483-501.

25. Ortega-Calvo, J. J.; Jimenez-Sanchez, C.; Pratarolo, P.; Pullin, H.; Scott, T. B.; Thompson, I. P. Tactic response of bacteria to zero-valent iron nanoparticles. *Environ. Pollut.* **2016,** *213*, 438-445.

Figure legend

FIGURE 1. A, C and E: Experimental results on NAH mineralization and transport of *Pseudomonas putida* G7 cells in percolated sand columns. The columns received a suspension of cells exhibiting intrinsic motility (1A), a negative tactic motility pattern in the presence of silver nanoparticles at 0.2 mg L^{-1} (1B), and a positive tactic motility pattern in the presence of sunflower root exudates at 16 mg L^{-1} of organic carbon (1C). The symbols represent the normalized outflow concentration of cells (●), total ^{14}C expressed as NAH equivalents $C_{tot,n}$ (□) and NAH equivalents converted into CO_2, $C_{CO2,n}$ (■) in the column effluent. Data are presented as means of determinations in duplicate columns. Error bars represent one standard deviation. B, D and F: Specific rates of NAH mineralization at given pore volumes (V_s, ■) and biomass of suspended (X_{sus}, ▲) and sand-attached bacteria (X_{att}, ●), calculated from the experimental results shown in the respective panels to the right. Data are presented as means of calculated values in duplicate columns.

21

461 FIGURE 1

462

463

464

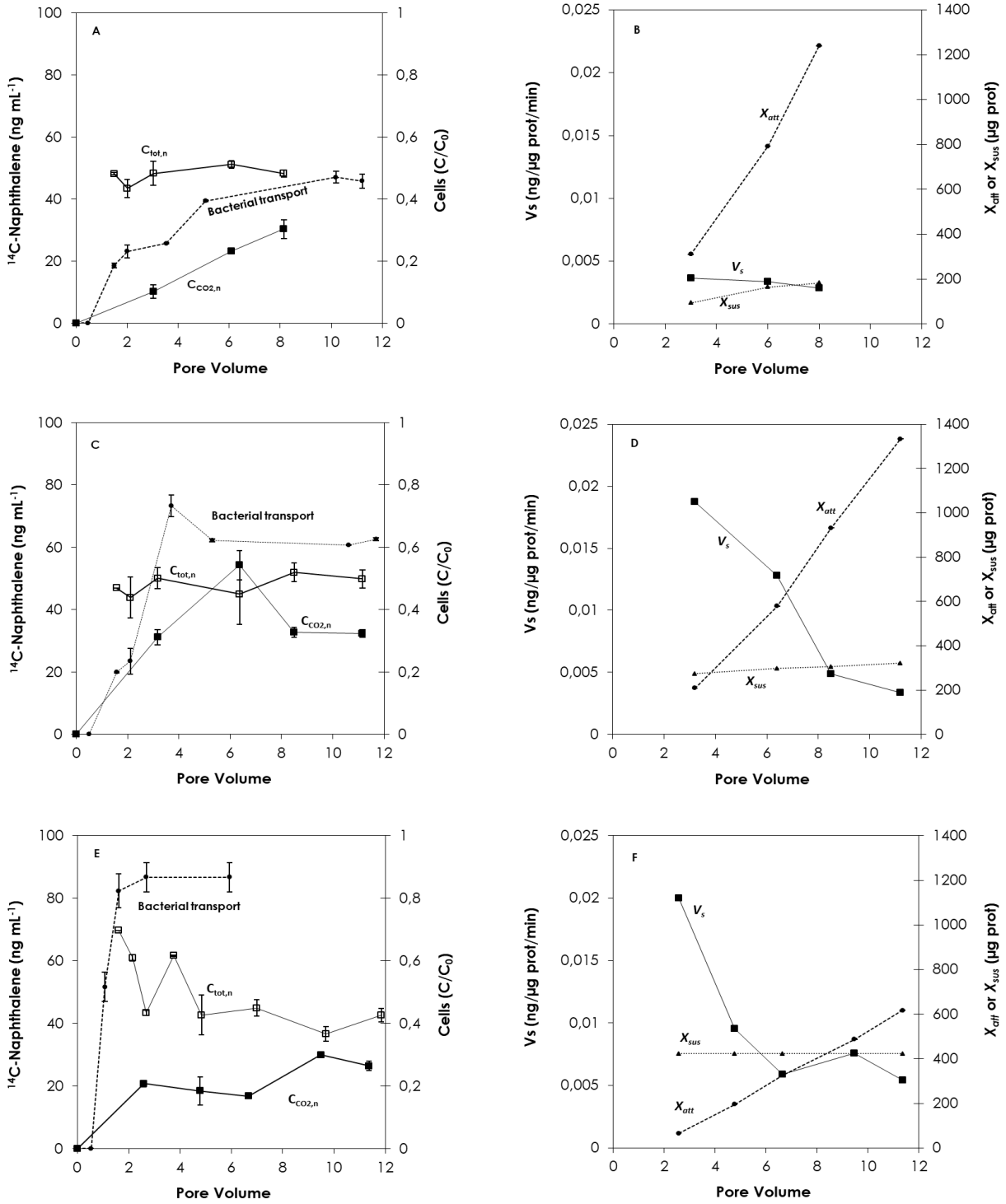

465

TABLE 1. Influence of motility patterns of *Pseudomonas putida* G7 cells on deposition, transport and naphthalene mineralization in batch experiments or during transport in saturated sand-filled columns.

		Batch Experiments				Column Experiments					
Motility (Treatment)	Turning events [a,b,c]	Adhesion[d] (%)		Naphthalene Mineralization[b]		Naphthalene Mineralization[b]		Deposition and transport [c]			
		Sand [c]	Silicone	V_s [e] (ng μg $_{prot}^{-1}$min^{-1})	E_{min} [f] (%)	V_s [g] (ng μg $_{prot}^{-1}$min^{-1})	E_{min} [h] (%)	X_{sus} /X_{att} [i]	PV[j]	α_0 [k]	B_f [l]
Control (intrinsic)	51 ± 1	38 ± 2	46 [m]	0.025 ± 0.003	44 ± 4	0.004 [m] 0.002 [m]	21 ± 10 41 ± 3	0.30 0.14	3.0 8.0	0.38	0.33
Negative taxis (AgNPs)	114 ± 3	58 ± 4	55 ± 2	0.017 ± 0.005	34 ± 5	0.017 ± 0.001 0.005 [m]	56 ± 18 79 ± 0	1.31 0.32	3.2 8.5	0.60	0.70
Positive taxis (Root exudates)	13 [m]	9 ± 1	31 ± 2	0.022 ± 0.003	42 ± 4	0.020 ± 0.005 0.006 ± 0.001	33 ± 4 35 ± 7	6.50 1.30	2.6 6.7	0.18	1.20

[a] Total number of turning events (rate of change of direction greater than 1,000 s^{-1}); [b] Values are reported as mean ± one standard deviation; [c] Data from previous publications; [9, 12] [d] Percentage of cells adhered to sand or silicone pieces in batch experiments; [e] V_s, specific mineralization rate; [f] Mineralization extent; [g] V_s value in column experiments at PV as defined in the column 'PV'; [h] Percentage of leached naphthalene mineralized at PV defined in the column 'PV'; [i] X_{sus} / X_{att}, biomass ratio of suspended to attached bacteria at PV as defined in the column 'PV'; [j] PV, pore volume; [k] adhesion efficiency; [l] Blocking factor. [m] Standard Deviation <0.1%;

23